Chapter 12
Protection of Nine-Phase Transmission Line Using Biorthogonal-2.2 Wavelet Transform

Gaurav Kapoor

1 Introduction

An increase in the inevitability of electrical power has been perceived by the people of the modern generation. The electrical power transfer potentiality of the currently operating power transmission systems ought to be augmented in order to assist the significant increase in the necessity of electrical energy. In the literature, NPTL's have been suggested as an imminent replacement of the prevalent configuration of the electrical power transmission system which has the prospective for transferring the large extent of electrical energy.

The feasibility of fault occurrence on the NPTL is more as compared with the DCTL. Thus, accurate recognition of the faults in the NPTL turns out to be very decisive for mitigating the loss of gain and providing fast renovates.

Several newly reported research works addressed the issue related to fault recognition and categorization in TL's. Some important research attempts are presented in concise here in this section. Recently, fuzzy logic has been employed for micro-grid protection [1]. The TPTL has been protected using WT in [2]. In [3], ConvNet has been applied for fault recognition in micro-grid. In [4, 5], WT has been used for fault categorization in SPTL and SCCDCTL, respectively. Mathematical morphology has been applied for SPTL protection in [6]. ANN and phasor data have been used for islanding recognition in the smart grid [7]. HHT has been used for SPTL protection in [8]. In [9], POVMD and WPNRVFLN have been employed for fault recognition in SCDCTL. Mathematical morphology and data mining-based techniques have been used for high impedance recognition [10].

In this work, a novel tool, i.e., the biorthogonal-2.2 wavelet transform (BWT) is used for NPTL protection. No such type of work has been reported yet to the

G. Kapoor (✉)
Modi Institute of Technology, Kota, India
e-mail: gaurav.kapoor019@gmail.com

M. Shorif Uddin et al. (eds.), *Intelligent Energy Management Technologies*, Algorithms for Intelligent Systems,
https://doi.org/10.1007/978-981-15-8820-4_12

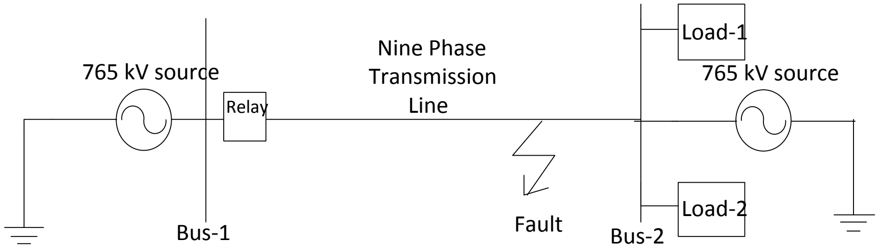

Fig. 1 The graphic of 765 kV nine-phase power system

best of the knowledge of the author. The results show that the BWT powerfully recognizes and categorizes the faults and the consistency of BWT is not perceptive to the variation in various fault factors.

This article is structured as: The specifications of NPTL are reported in Sect. 2. Section 3 shows the flow diagram of BWT. Section 4 is dedicated to the discussion of the response of BWT. Section 5 completes the paper.

2 The Specifications of NPTL

The system of a 765 kV NPTL is designed using MATLAB. Figure 1 shows the illustration of NPTL. The NPTL has a rating of 765 kV, 50 Hz, and has a total length of 200 km. The NPTL is separated into two zones of length 100 km both. Two loads of 300 MW and 150 MVAr each are connected at the receiving end of NPTL. The combination of relay and transducers is connected near bus-1 for the relaying of the total length of NPTL.

3 BWT-Based Protection Technique

Figure 2 shows the process of BWT with the following steps:

Step-1 Nine-phase currents are recorded through transducers installed at bus-1.
Step-2 BWT is employed to estimate the BWT outputs of phase currents.
Step-3 The phase will be declared as the faulty phase if its BWT output has a larger amplitude as compared to the output of the healthy phase under a faulty situation.

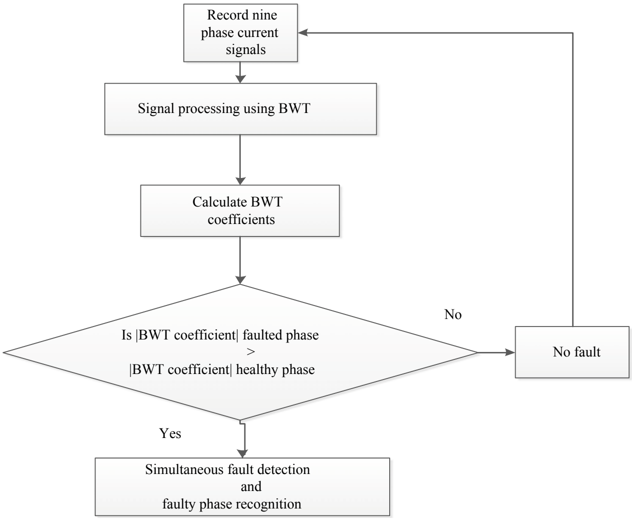

Fig. 2 Flow chart of BWT

4 Performance Assessment

To substantiate the ability of the BWT, the simulation effort has been carried out for numerous faults. The simulation outcomes of the study are examined in the successive subsections.

4.1 Response of BWT for Healthy Situation

Figure 3 shows the nine-phase currents and voltages for no-fault. Figure 4 exemplifies the output of BWT for no-fault. Table 1 reports the results of BWT for no-fault.

4.2 Response of BWT for Fault Switching Time Variation

The BWT is investigated for variation in fault switching time (FST). Figure 5 depicts the ABCEGHI-g fault at 100 km at 0.05 s among $R_F = 2.15\ \Omega$ and $R_G = 3.15\ \Omega$. Figure 6 shows the output of BWT for the ABCEGHI-g fault simulated at 0.05 s. The fault factors for all the fault cases are set as: T = 0.05 s, $F_L = 100$ km, $R_F = 2.15\ \Omega$, and $R_G = 3.15\ \Omega$. Tables 2, 3, 4, 5, and 6 tabularizes the results for variation in FST. It is inspected from Tables 2, 3, 4, 5, and 6 that the variation in FST does not manipulate the operation of BWT.

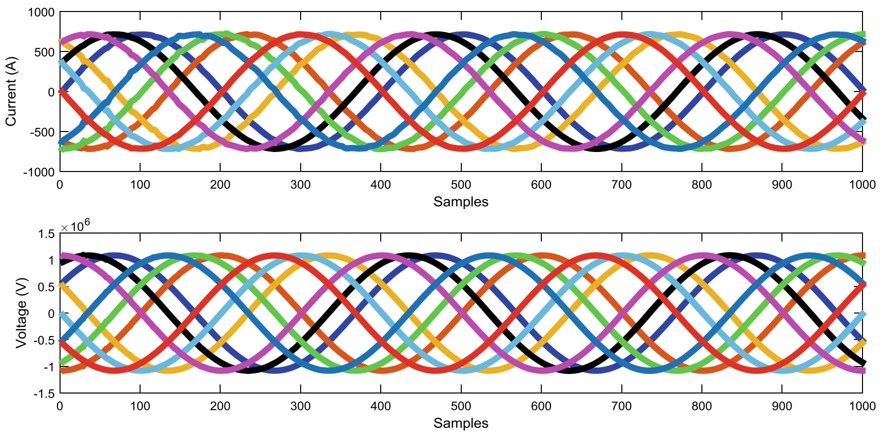

Fig. 3 Nine-phase currents and voltages for no-fault

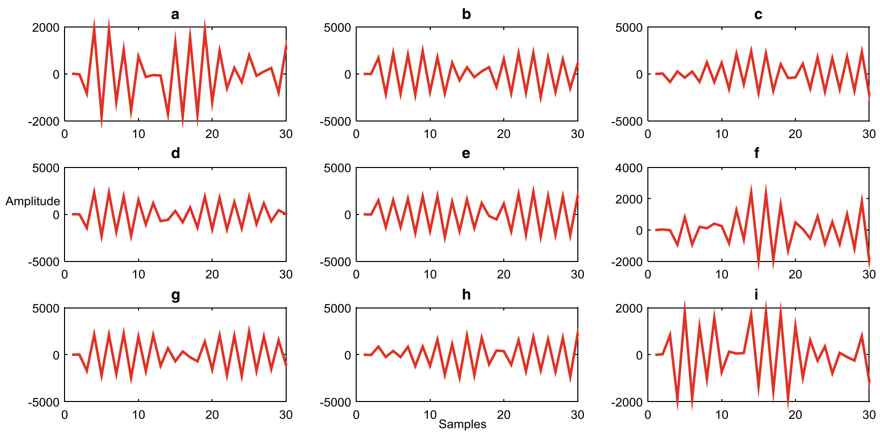

Fig. 4 BWT outputs for no-fault

Table 1 Response of BWT for no-fault

BWT outputs		
Phase-A	Phase-B	Phase-C
2.1264×10^3	2.4245×10^3	2.3967×10^3
Phase-D	Phase-E	Phase-F
2.3212×10^3	2.3690×10^3	2.3704×10^3
Phase-G	Phase-H	Phase-I
2.4514×10^3	2.1949×10^3	2.1032×10^3

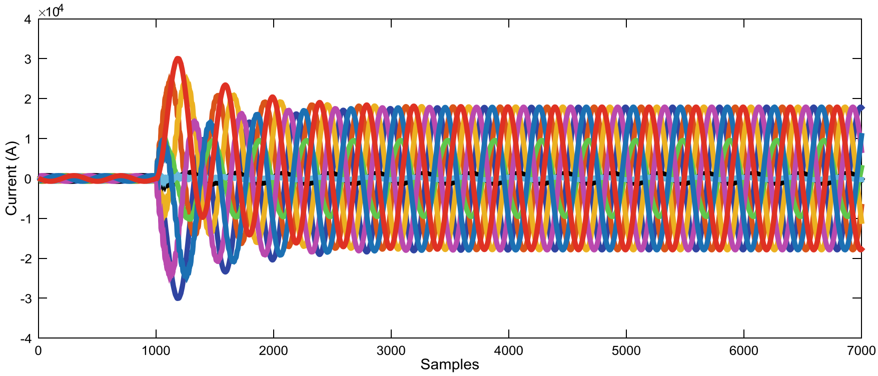

Fig. 5 ABCEGHI-g fault at 100 km at 0.05 s among $R_F = 2.15\ \Omega$ and $R_G = 3.15\ \Omega$

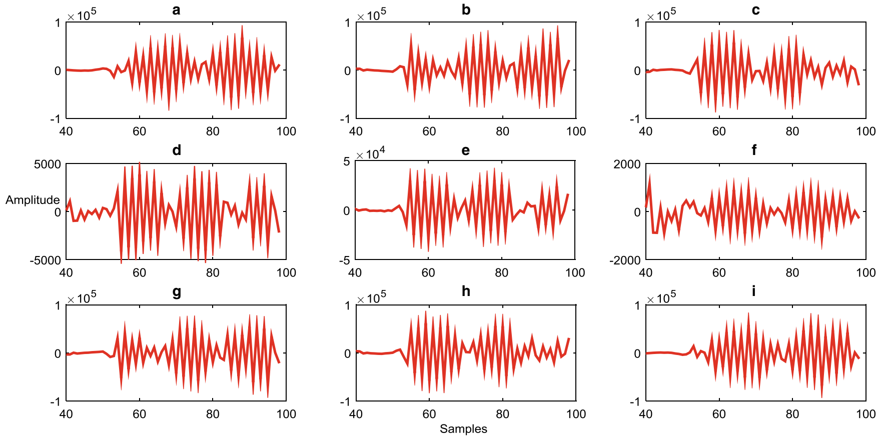

Fig. 6 BWT outputs for ABCEGHI-g fault at 100 km at 0.05 s among $R_F = 2.15\ \Omega$ and $R_G = 3.15\ \Omega$

Table 2 Response of BWT for ABCEGHI-g fault at 100 km at 0.05 s among $R_F = 2.15\ \Omega$ and $R_G = 3.15\ \Omega$

Fault—ABCEGHI-g (FST = 0.05 s)					
Phase	BWT output	Phase	BWT output	Phase	BWT output
A	6.7582×10^4	D	3.8703×10^3	G	5.4475×10^4
B	6.7227×10^4	E	3.0215×10^4	H	6.1760×10^4
C	5.7644×10^4	F	2.3550×10^3	I	5.8108×10^4

Table 3 Response of BWT for ABGHI-g fault at 100 km at 0.1 s among $R_F = 2.15\ \Omega$ and $R_G = 3.15\ \Omega$

Fault—ABGHI-g (FST = 0.1 s)					
Phase	BWT output	Phase	BWT output	Phase	BWT output
A	5.7034×10^4	D	2.1756×10^3	G	6.2186×10^4
B	5.4816×10^4	E	2.3311×10^3	H	5.4787×10^4
C	2.5569×10^3	F	2.4938×10^3	I	6.1941×10^4

Table 4 Response of BWT for BCDEF-g fault at 100 km at 0.17 s among $R_F = 2.15\ \Omega$ and $R_G = 3.15\ \Omega$

Fault—BCDEF-g (FST = 0.17 s)					
Phase	BWT output	Phase	BWT output	Phase	BWT output
A	2.8030×10^3	D	6.3673×10^4	G	2.3346×10^3
B	5.4067×10^4	E	6.0301×10^4	H	2.5046×10^3
C	5.2134×10^4	F	5.9313×10^4	I	2.3395×10^3

Table 5 Response of BWT for ABHI-g fault at 100 km at 0.08 s among $R_F = 2.15\ \Omega$ and $R_G = 3.15\ \Omega$

Fault—ABHI-g (FST = 0.08 s)					
Phase	BWT output	Phase	BWT output	Phase	BWT output
A	5.5787×10^4	D	2.3102×10^3	G	2.6451×10^3
B	4.9309×10^4	E	2.3134×10^3	H	5.3814×10^4
C	2.6365×10^3	F	2.4714×10^3	I	4.5725×10^4

Table 6 Response of BWT for DEF-g fault at 100 km at 0.2 s among $R_F = 2.15\ \Omega$ and $R_G = 3.15\ \Omega$

Fault—DEF-g (FST = 0.2 s)					
Phase	BWT output	Phase	BWT output	Phase	BWT output
A	2.3810×10^3	D	5.6832×10^4	G	2.3544×10^3
B	2.1445×10^3	E	5.9226×10^4	H	2.2560×10^3
C	2.1369×10^3	F	5.7041×10^4	I	2.4192×10^3

4.3 Response of BWT for Near-in Relay Faults

The efficiency of the BWT is tested for various near-in relay faults on the NPTL. Figure 7 depicts the DEFGHI-g near-in relay fault current at 5 km at 0.12 s among $R_F = 3.5\ \Omega$ and $R_G = 2.5\ \Omega$. Figure 8 shows the BWT coefficients for the DEFGHI-g fault simulated at 5 km. The fault factors for all the fault cases are: T = 0.12 s, $R_F = 3.5\ \Omega$ and $R_G = 2.5\ \Omega$. Tables 7, 8, 9, 10, and 11 details the results of the BWT for

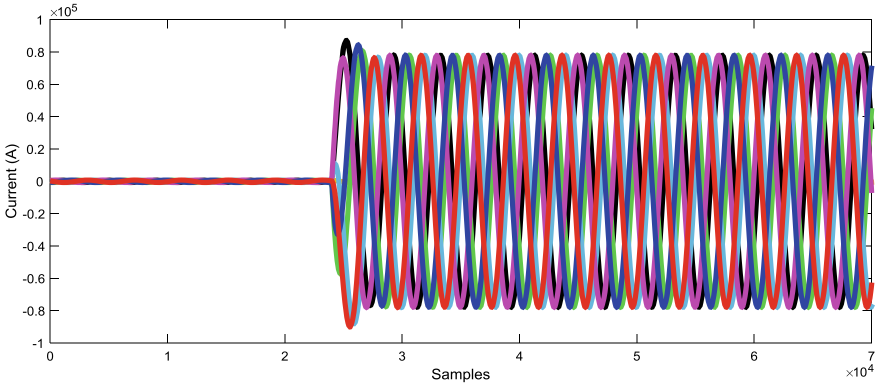

Fig. 7 DEFGHI-g near-in relay fault at 5 km at 0.12 s among $R_F = 3.5\ \Omega$ and $R_G = 2.5\ \Omega$

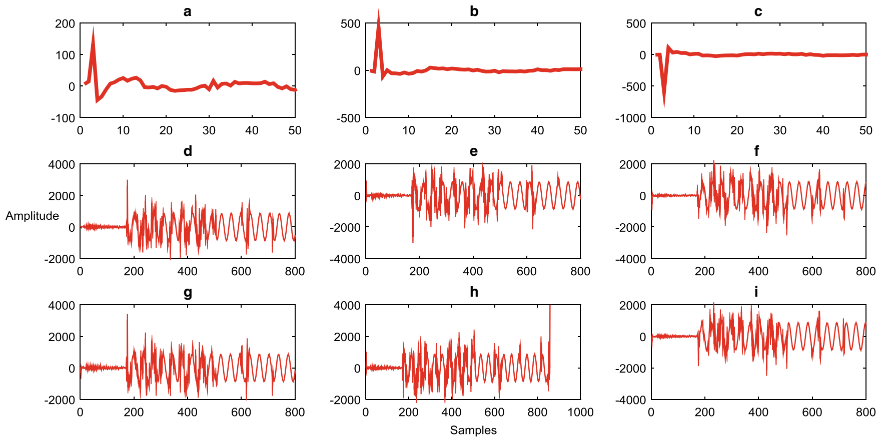

Fig. 8 BWT outputs for DEFGHI-g near-in fault at 5 km among $R_F = 3.5\ \Omega$ and $R_G = 2.5\ \Omega$

Table 7 Response of BWT for DEFGHI-g fault at 5 km

Fault—DEFGHI-g (5 km)					
Phase	BWT output	Phase	BWT output	Phase	BWT output
A	131.6663	D	2.6131×10^3	G	3.0297×10^3
B	456.0025	E	6.5031×10^3	H	3.9445×10^3
C	108.0168	F	1.8497×10^3	I	3.3792×10^3

five different near-in relay faults. It is confirmed from Tables 7, 8, 9, 10, and 11 that the BWT has the ability to detect the near-in relay faults precisely.

Table 8 Response of BWT for ABCEF-g fault at 6 km

Fault—ABCEF-g (6 km)					
Phase	BWT output	Phase	BWT output	Phase	BWT output
A	3.0852×10^3	D	818.7633	G	26.7045
B	9.0172×10^3	E	6.2284×10^3	H	194.3373
C	2.6214×10^3	F	2.5241×10^3	I	93.5313

Table 9 Response of BWT for GHI-g fault at 7 km

Fault—GHI-g (7 km)					
Phase	BWT output	Phase	BWT output	Phase	BWT output
A	86.5409	D	30.4280	G	5.1182×10^3
B	299.8279	E	394.6009	H	5.2485×10^3
C	89.1173	F	87.1063	I	3.5345×10^3

Table 10 Response of BWT for ABC-g fault at 8 km

Fault—ABC-g (8 km)					
Phase	BWT output	Phase	BWT output	Phase	BWT output
A	2.9549×10^3	D	61.3253	G	65.5750
B	1.0461×10^3	E	272.2014	H	249.4814
C	2.9781×10^3	F	81.4085	I	104.3835

Table 11 Response of BWT for DEF-g fault at 9 km

Fault—DEF-g (9 km)					
Phase	BWT output	Phase	BWT output	Phase	BWT output
A	106.9428	D	5.0679×10^3	G	94.3637
B	312.8468	E	8.8515×10^3	H	389.2334
C	173.8100	F	3.4420×10^3	I	103.6978

4.4 Response of BWT for Far-End Relay Faults

The BWT has been explored for different far-end relay faults. Figure 9 illustrates the ABCDEFG-g far-end relay fault at 195 km at 0.06 s among $R_F = 4.5\ \Omega$ and $R_G = 3.5\ \Omega$. Figure 10 shows the BWT coefficients for the ABCDEFG-g fault simulated at 195 km. The fault factors chosen for all the fault cases are: $T = 0.06$ s, $R_F = 4.5\ \Omega$ and $R_G = 3.5\ \Omega$. Tables 12, 13, 14, 15, and 16 report the results for various far-end relay faults. It is inspected from Tables 12, 13, 14, 15, and 16 that the effectiveness of BWT remains impassive for different far-end relay faults.

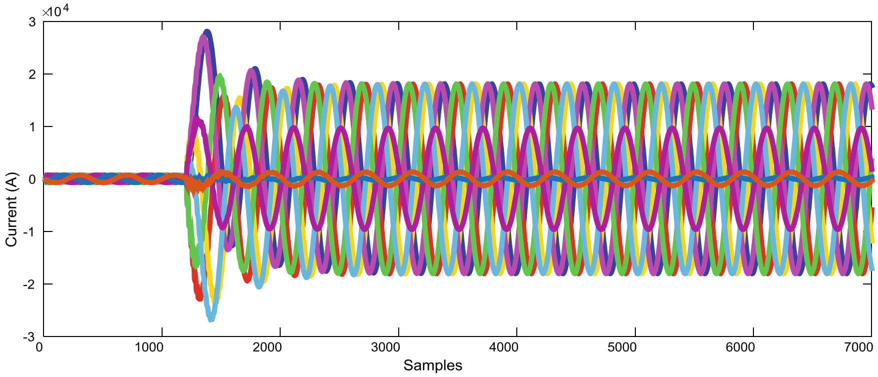

Fig. 9 ABCDEFG-g fault at 195 km at 0.06 s among $R_F = 4.5\ \Omega$ and $R_G = 3.5\ \Omega$

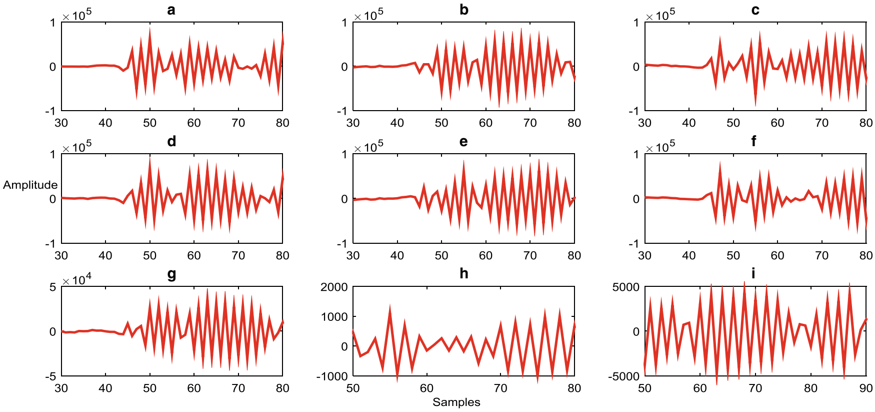

Fig. 10 BWT outputs for ABCDEFG-g fault at 195 km at 0.06 s among $R_F = 4.5\ \Omega$ and $R_G = 3.5\ \Omega$

Table 12 Response of BWT for ABCDEFG-g fault at 195 km

Fault—ABCDEFG-g (195 km)					
Phase	BWT output	Phase	BWT output	Phase	BWT output
A	6.1249×10^4	D	6.6442×10^4	G	3.4487×10^4
B	5.9615×10^4	E	6.1556×10^4	H	2.1853×10^3
C	5.3307×10^4	F	5.7471×10^4	I	4.2411×10^3

4.5 *Response of BWT for Variation in Fault Resistance*

The BWT is investigated for variation in fault resistances. Figure 11 depicts the ABCDEFHI-g fault at 100 km at 0.07 s among $R_F = 10\ \Omega$ and $R_G = 0.001\ \Omega$.

Table 13 Response of BWT for ABDEF-g fault at 196 km

Fault—ABDEF-g (196 km)					
Phase	BWT output	Phase	BWT output	Phase	BWT output
A	5.3989×10^4	D	5.7792×10^4	G	2.4971×10^3
B	4.7741×10^4	E	5.9487×10^4	H	2.3224×10^3
C	2.8607×10^3	F	5.9446×10^4	I	2.4280×10^3

Table 14 Response of BWT for EFGHI-g fault at 197 km

Fault—EFGHI-g (197 km)					
Phase	BWT output	Phase	BWT output	Phase	BWT output
A	2.3752×10^3	D	2.7792×10^3	G	6.1323×10^4
B	2.3674×10^3	E	5.0953×10^4	H	5.4694×10^4
C	2.1085×10^3	F	4.8050×10^4	I	5.5860×10^4

Table 15 Response of BWT for ABDE-g fault at 198 km

Fault—ABDE-g (198 km)					
Phase	BWT output	Phase	BWT output	Phase	BWT output
A	5.6799×10^4	D	5.5657×10^4	G	2.2046×10^3
B	5.1894×10^4	E	4.9065×10^4	H	2.4423×10^3
C	2.5343×10^3	F	2.5271×10^3	I	2.3698×10^3

Table 16 Response of BWT for ABC-g fault at 199 km

Fault—ABC-g (199 km)					
Phase	BWT output	Phase	BWT output	Phase	BWT output
A	5.9040×10^4	D	2.1843×10^3	G	2.1728×10^3
B	5.5764×10^4	E	2.3957×10^3	H	2.2799×10^3
C	5.1070×10^4	F	2.2733×10^3	I	2.1238×10^3

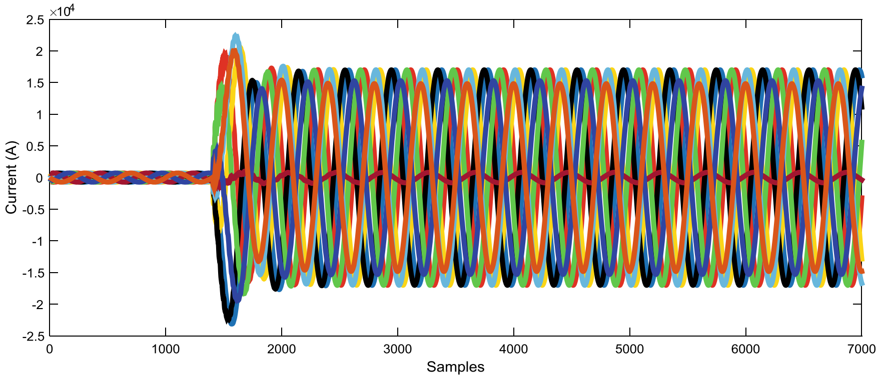

Fig. 11 ABCDEFHI-g fault at 0.07 s at 100 km among $R_F = 10\ \Omega$ and $R_G = 0.001\ \Omega$

Figure 12 shows the BWT coefficients for the ABCDEFHI-g fault simulated among $R_F = 10\ \Omega$. The fault factors for all the fault cases are set as $T = 0.07$ s, $F_L = 100$ km, and $R_G = 0.001\ \Omega$. Tables 17, 18, 19, 20, and 21 tabularizes the results for variation in fault resistances. It is inspected from Tables 17, 18, 19, 20, and 21 that variation in the fault resistances does not manipulate the working of the BWT.

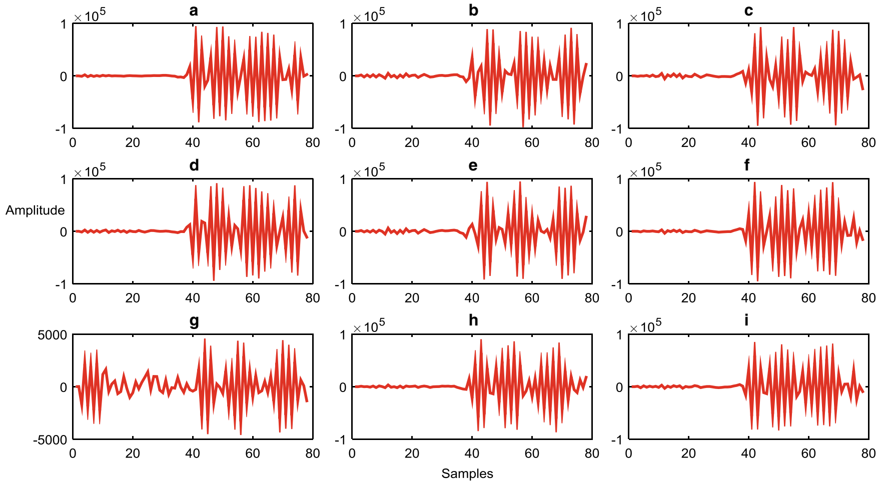

Fig. 12 BWT outputs for ABCDEFHI-g fault at 0.07 s at 100 km among $R_F = 10\ \Omega$ and $R_G = 0.001\ \Omega$

Table 17 Response of BWT for ABCDEFHI-g fault among $R_F = 10\ \Omega$

Fault—ABCDEFHI-g (10 Ω)					
Phase	BWT output	Phase	BWT output	Phase	BWT output
A	6.8829×10^4	D	6.5690×10^4	G	3.2895×10^3
B	6.5526×10^4	E	6.8908×10^4	H	6.4465×10^4
C	6.7075×10^4	F	6.7971×10^4	I	5.9149×10^4

Table 18 Response of BWT for BCDEF-g fault among $R_F = 40\ \Omega$

Fault—BCDEF-g (40 Ω)					
Phase	BWT output	Phase	BWT output	Phase	BWT output
A	2.7621×10^3	D	3.8084×10^4	G	2.2360×10^3
B	3.2730×10^4	E	3.6160×10^4	H	2.3975×10^3
C	3.3935×10^4	F	3.9879×10^4	I	2.3335×10^3

Table 19 Response of BWT for ACGH-g fault among $R_F = 70\ \Omega$

Fault—ACGH-g (70 Ω)					
Phase	BWT output	Phase	BWT output	Phase	BWT output
A	2.6259×10^4	D	2.4778×10^3	G	2.4334×10^4
B	3.0921×10^3	E	2.5364×10^3	H	2.8309×10^4
C	2.5700×10^4	F	2.2849×10^3	I	2.6976×10^3

Table 20 Response of BWT for DEF-g fault among $R_F = 100\ \Omega$

Fault—DEF-g (100 Ω)					
Phase	BWT output	Phase	BWT output	Phase	BWT output
A	2.2718×10^3	D	1.9765×10^4	G	2.3222×10^3
B	2.2663×10^3	E	1.8950×10^4	H	2.3157×10^3
C	2.3288×10^3	F	1.9448×10^4	I	2.1198×10^3

Table 21 Response of BWT for AGHI-g fault among $R_F = 150\ \Omega$

Fault—AGHI-g (150 Ω)					
Phase	BWT output	Phase	BWT output	Phase	BWT output
A	1.7154×10^4	D	2.4446×10^3	G	2.0733×10^4
B	2.2694×10^3	E	2.2100×10^3	H	1.9942×10^4
C	3.1200×10^3	F	2.4650×10^3	I	2.1785×10^4

5 Conclusion

This work showed an improved revelation using BWT to recognize and categorize the faults occurring on NPTL. The BWT coefficients of the nine-phase currents of the NPTL which are measured at one-end are employed by BWT for fault recognition, categorization, and faulty phase identification. The value of fault resistance is varied from 10 to 150 Ω, the position of fault for the near-in relay faults is varied from 5 to 9 km, and the position of fault for the far-end relay faults is varied from 195 to 199 km. The simulation studies support the consistency of BWT under extensive variations in fault type, location, resistance, and switching time. From the results, it is noticeable that there is an evident intolerance between the fault and no-fault situations and establishes the potential of the BWT-based fault recognition and faulty phase categorization technique by recognizing the faults correctly.

References

1. Chaitanya BK, Soni AK, Yadav A (2018) Communication assisted fuzzy based adaptive protective relaying scheme for microgrid. J Power Technol 98(1):57–69
2. Kapoor G (2018) Wavelet transform based detection and classification of multi-location three phase to ground faults in twelve phase transmission line. Majlesi J Mechatron Systems 7(4):47–60
3. Manohar M, Koley E, Ghosh S (2019) Enhancing resilience of PV-fed microgrid by improved relaying and differentiating between inverter faults and distribution line faults. Electric Power Energy Syst (Elsevier) 108:271–279
4. Kapoor G (2018) Six phase transmission line boundary protection using wavelet transform. In: Proceedings of the 8th IEEE India international conference on power electronics (IICPE). IEEE. Jaipur, India (2018)
5. Gautam N, Ali S, Kapoor G (2018) Detection of fault in series capacitor compensated double circuit transmission line using wavelet transform. In: Proceedings of the IEEE international conference on computing, power and communication technologies (GUCON), pp 769–773. IEEE. Greater Noida, India (2018)
6. Kapoor G (2018) Six phase transmission line boundary protection using mathematical morphology. In: Proceedings of the IEEE international conference on computing, power and communication technologies (GUCON), pp 857–861. IEEE. Greater Noida, India (2018)
7. Kumar D, Bhowmik PS (2018) Artificial neural network and phasor data-based islanding detection in smart grid. IET Gener Transm Distrib 12(21):5843–5850
8. Kapoor G (2019) Detection and classification of single line to ground boundary faults in a 138 kV six phase transmission line using Hilbert Huang transform. i-manager's J Electric Eng 12(3):28–41 (2019)
9. Sahani M, Dash P K (2019) Fault location estimation for series-compensated double-circuit transmission line using parameter optimized variational mode decomposition and weighted P-norm random vector functional link network. Appl Soft Comput J (Elsevier), 1–18 (2019)
10. Sekar K, Mohanty NK (2018) Data mining-based high impedance fault detection using mathematical morphology. Comput Electric Eng (Elsevier) 69:129–141